VOLUME 101 | SUPPLEMENT 1 | MARCH 2021

LI

LABORATORY INVESTIGATION

THE BASIC AND TRANSLATIONAL PATHOLOGY RESEARCH JOURNAL

ABSTRACTS

PATHOBIOLOGY AND EMERGING TECHNIQUES (891-902)

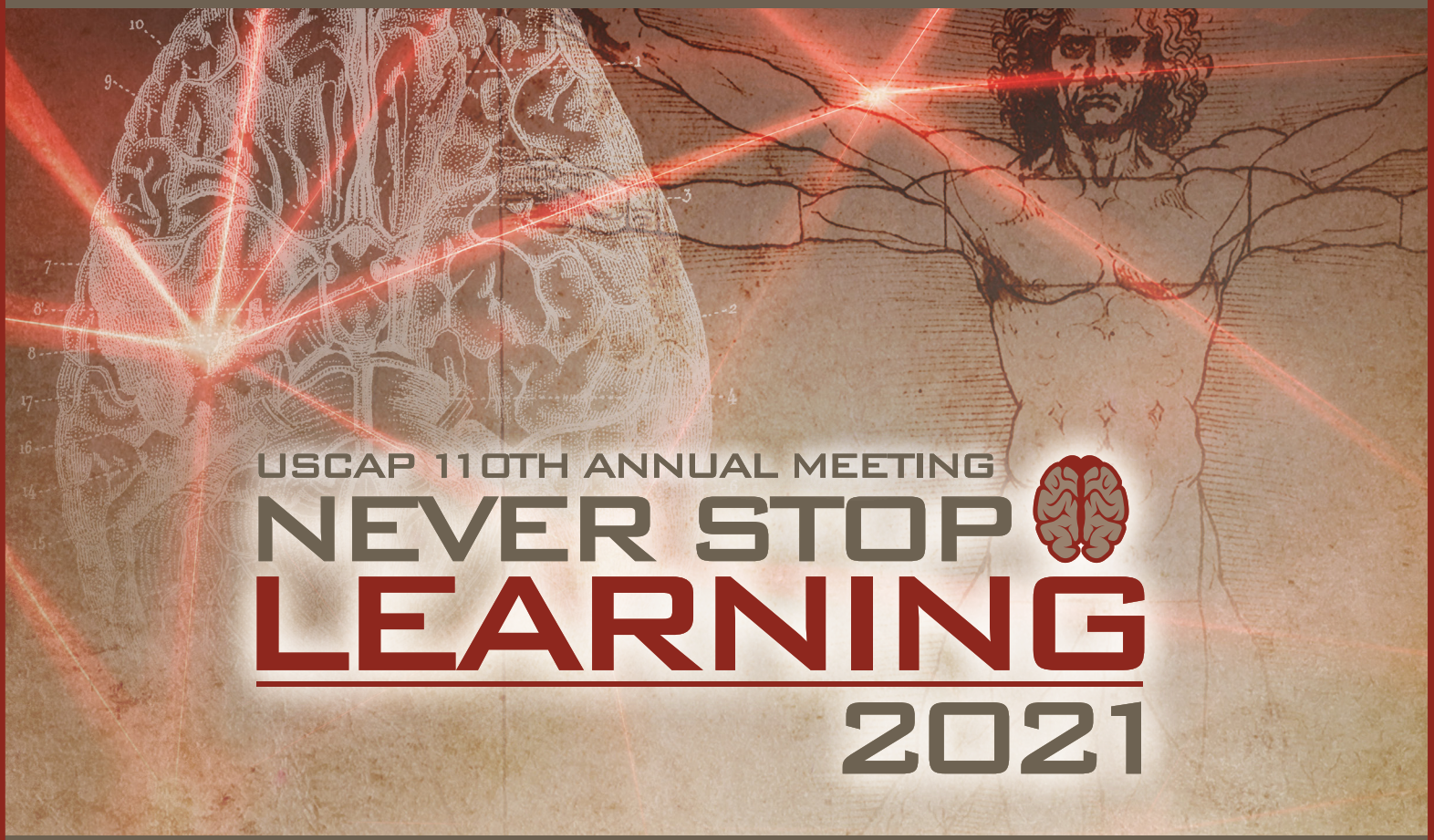

MARCH 13-18, 2021 | VIRTUAL AND INTERACTIVE

Published by
SPRINGER NATURE
www.ModernPathology.org

USCAP
Creating a Better Pathologist
AN OFFICIAL JOURNAL OF THE UNITED STATES AND CANADIAN ACADEMY OF PATHOLOGY

EDUCATION COMMITTEE

Jason L. Hornick
Chair

Rhonda K. Yantiss, Chair
Abstract Review Board and Assignment Committee

Kristin C. Jensen
Chair, CME Subcommittee

Laura C. Collins
Interactive Microscopy Subcommittee

Raja R. Seethala
Short Course Coordinator

Ilan Weinreb
Subcommittee for Unique Live Course Offerings

David B. Kaminsky
(Ex-Officio)
Zubair W. Baloch
Daniel J. Brat
Sarah M. Dry
William C. Faquin
Yuri Fedoriw
Karen Fritchie
Jennifer B. Gordetsky
Melinda Lerwill
Anna Marie Mulligan
Liron Pantanowitz
David Papke,
Pathologist-in-Training
Carlos Parra-Herran
Rajiv M. Patel
Deepa T. Patil
Charles Matthew Quick
Lynette M. Sholl
Olga K. Weinberg
Maria Westerhoff
Nicholas A. Zoumberos,
Pathologist-in-Training

ABSTRACT REVIEW BOARD

Benjamin Adam
Rouba Ali-Fehmi
Daniela Allende
Ghassan Allo
Isabel Alvarado-Cabrero
Catalina Amador
Tatjana Antic
Roberto Barrios
Rohit Bhargava
Luiz Blanco
Jennifer Boland
Alain Borczuk
Elena Brachtel
Marilyn Bui
Eric Burks
Shelley Caltharp
Wenqing (Wendy) Cao
Barbara Centeno
Joanna Chan
Jennifer Chapman
Yunn-Yi Chen
Hui Chen
Wei Chen
Sarah Chiang
Nicole Cipriani
Beth Clark
Alejandro Contreras
Claudiu Cotta
Jennifer Cotter
Sonika Dahiya
Farbod Darvishian
Jessica Davis
Heather Dawson
Elizabeth Demicco
Katie Dennis
Anand Dighe
Suzanne Dintzis
Michelle Downes
Charles Eberhart
Andrew Evans
Julie Fanburg-Smith
Michael Feely
Dennis Firchau
Gregory Fishbein
Andrew Folpe
Larissa Furtado
Billie Fyfe-Kirschner
Giovanna Giannico
Christopher Giffith
Anthony Gill
Paula Ginter
Tamar Giorgadze
Purva Gopal
Abha Goyal
Rondell Graham
Alejandro Gru
Nilesh Gupta
Mamta Gupta
Gillian Hale
Suntrea Hammer
Malini Harigopal
Douglas Hartman
Kammi Henriksen
John Higgins
Mai Hoang
Aaron Huber
Doina Ivan
Wei Jiang
Vickie Jo
Dan Jones
Kirk Jones
Neerja Kambham
Dipti Karamchandani
Nora Katabi
Darcy Kerr
Francesca Khani
Joseph Khoury
Rebecca King
Veronica Klepeis
Christian Kunder
Steven Lagana
Keith Lai
Michael Lee
Cheng-Han Lee
Madelyn Lew
Faqian Li
Ying Li
Haiyan Liu
Xiuli Liu
Lesley Lomo
Tamara Lotan
Sebastian Lucas
Anthony Magliocco
Kruti Maniar
Brock Martin
Emily Mason
David McClintock
Anne Mills
Richard Mitchell
Neda Moatamed
Sara Monaco
Atis Muehlenbachs
Bita Naini
Dianna Ng
Tony Ng
Michiya Nishino
Scott Owens
Jacqueline Parai
Avani Pendse
Peter Pytel
Stephen Raab
Stanley Radio
Emad Rakha
Robyn Reed
Michelle Reid
Natasha Rekhtman
Jordan Reynolds
Andres Roma
Lisa Rooper
Avi Rosenberg
Esther (Diana) Rossi
Souzan Sanati
Gabriel Sica
Alexa Siddon
Deepika Sirohi
Kalliopi Siziopikou
Maxwell Smith
Adrian Suarez
Sara Szabo
Julie Teruya-Feldstein
Khin Thway
Rashmi Tondon
Jose Torrealba
Gary Tozbikian
Andrew Turk
Evi Vakiani
Christopher VandenBussche
Paul VanderLaan
Hannah Wen
Sara Wobker
Kristy Wolniak
Shaofeng Yan
Huihui Ye
Yunshin Yeh
Anjana Yeldandi
Gloria Young
Lei Zhao
Minghao Zhong
Yaolin Zhou
Hongfa Zhu

To cite abstracts in this publication, please use the following format: **Author A, Author B, Author C, et al. Abstract title (abs#). In "File Title."** ***Laboratory Investigation*** **2021; 101 (suppl 1): page#**

891 Development of a Superior Method for the Reliable Expansion of Tumor-Infiltrating Natural Killer cells from Rare Human Malignancies for the Purposes of ex vivo Immunophenotyping and Immunotherapy

Saiaditya Badeti[1], Minh Ma[2], Pratik Deb[3], Albert Alhatem[2], Khalid Algarrahi[2], Pankaj Agarwalla[3], Dongfang Liu[4]

[1]Rutgers New Jersey Medical School, Newark, NJ, [2]Rutgers New Jersey Medical School/Rutgers University, Newark, NJ, [3]Rutgers New Jersey Medical School/University Hospital, Newark, NJ, [4]Rutgers Cancer Institute of New Jersey, Newark, NJ

Disclosures: Saiaditya Badeti: None; Minh Ma: None; Pratik Deb: None; Albert Alhatem: None; Khalid Algarrahi: None; Pankaj Agarwalla: None; Dongfang Liu: None

Background: Exploring the role of Tumor-Infiltrating Natural Killer (TINK) cells within the tumor microenvironment is a central component in the study of oncology and tumor-host interactions. The low numbers of obtainable cells from small tumor specimens represents a significant challenge in studying TINKs. Also, current platforms for culturing and propagating primary cells, *ex vivo*, are unable to expand TINKs from difficult tissues. Thus, a protocol for the successful isolation and expansion of TINKs is of dire need. To our knowledge, no previous study has shown successful and reliable expansion of TINK cells from small tumors from different tissues. Our objective was to investigate whether a newly developed NK expansion platform for blood sources could be used to derive TINKs.

Design: 4 different human tumor tissues were used to isolate and expand TINKs: Endometrial Carcinosarcoma, Glioblastoma, Hepatocellular Carcinoma, and Melanoma. Briefly, tumor tissue was digested to obtain single-cell suspensions which were then fractionated to obtain tumor-infiltrating lymphocytes (TILs). Then, using 721.221-mIL21 feeder cells developed in our lab, TILs were expanded for 14 days before staining with CD3 and CD56 to delineate human TINK populations using flow cytometry.

Results: Our protocol for the isolation and expansion of TINKs from 4 different types of tumors (<1cm) was successful and yielded between 59 and 96% purity (Fig. 1). This platform can expand TINK cells for over 1 month for downstream analyses. Additionally, for the endometrial carcinosarcoma sample, we evaluated the expansion capabilities of our 721.221-mIL21 feeder cells compared to a similar feeder cell, K562-mIL21. Astonishingly, a nearly 6-fold increase in the total NK cell numbers was observed using the 721.221-mIL21 feeder cells (Fig. 2). Specifically, 721.221-mIL21 expanded 6.3 million TINK cells (61% viability) compared to K562-mIL21 which expanded 1.4 million TINK cells (50% viability) by Day 14 suggesting that our platform can reliably expand TINK cells with higher yields and viabilities compared to existing protocols.

Figure 1 – 891

Figure 1

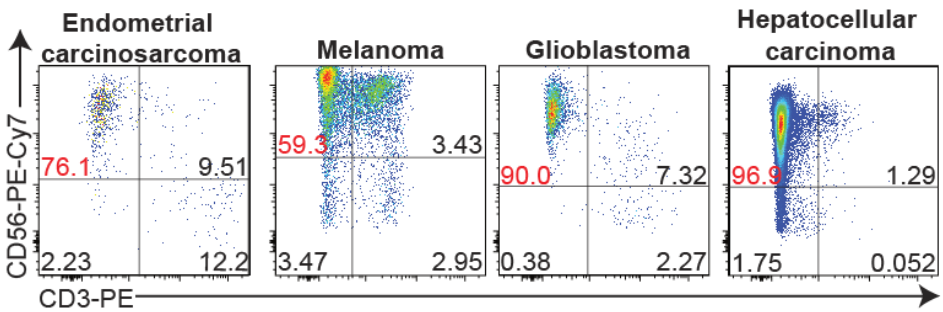

Figure 2 – 891

Figure 2

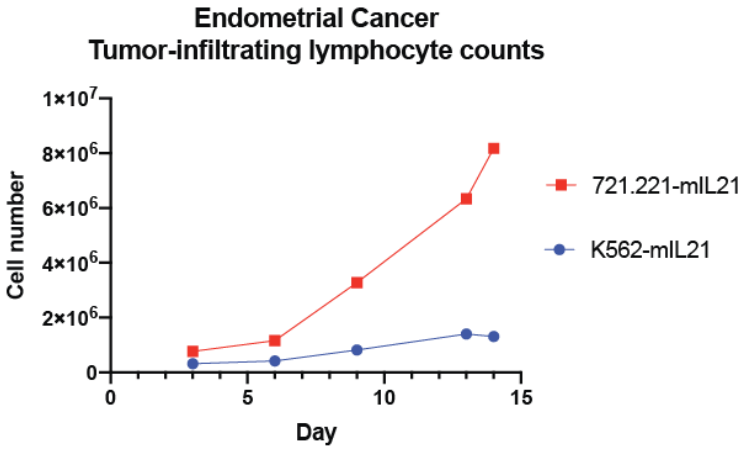

Conclusions: We provide a novel methodology for the *ex vivo* isolation and expansion of rare TINK populations. We also show that this technique can reliably and consistently increase total yields and viabilities of TINKs underscoring its use for long-term analyses involving rare malignancies. These results overcome a critical hurdle for pathologists and immunologists interested in TINK immunotherapy.

892 Mutational Signature in Hypermutated Malignant Neoplasms with Emphasis on Its Utility in Metastases of Unknown Primary: One Institutional Experience

Ruifeng (Ray) Guo[1], Jaime Davila[2], Zachary Fogarty[1], Chen Wang[3]
[1]Mayo Clinic, Rochester, MN, [2]Northfield, MN, [3]Mayo Clinic College of Medicine and Science, Rochester, MN

Disclosures: Ruifeng (Ray) Guo: None; Jaime Davila: None; Zachary Fogarty: None

Background: Clinical genomic mutation panels for cancer related genes have been widely applied in practice to look for actionable targets, especially for tumors of clinically advanced stage or the ones that are difficult to treat with conventional modalities. We systemically analyzed the mutational burden and gene signatures of all the samples (2016-2020) submitted for a large clinical cancer mutation panel from our institution, with focus on identification of hypermutated cases, potential utility in determining metastatic tumors of unknown primary and association with treatment response to immunotherapy.

Design: A total of 2442 cases were identified with the majority being metastatic tumors. All of them were submitted to a next generation sequencing-based large clinical cancer panel that covered approximately 0.8 megabases of the genome containing 324 genes (FoundationOne panel). Highly mutated cases were identified in this cohort and well suited for mutational signature profiling. Among them, clinical treatment with follow-up was incorporated for analysis in the ones submitted as metastases of unknown primary.

Results: 150/2442 cases were considered as highly mutated tumors, which can be classified into 4 main categories corresponding to COSMIC mutational signatures, including UV (n=61), deficient mismatch repair (MMR) (n=38), APOBEC (n=28) and tobacco (n=23). The signatures matched with corresponding tumor types when the primary sites were known. 27/150 cases were submitted as metastatic tumor of unknown primary. Among them, all cases of metastatic melanoma (12/12), metastatic squamous cell carcinoma of suspicious skin primary (4/4) and one case of suspicious metastatic Merkel cell carcinoma (1/1) showed UV signature, confirming skin primary. In addition, 3/4 metastatic carcinomas with tobacco signature had imaging findings supportive of pulmonary origin, and 1/2 metastatic carcinomas with APOBEC signatures had subsequent confirmed primary renal pelvic urothelial carcinoma. Interestingly, no primary sites were defined in three cases with MMR signature. Irrespective of tumor type, 21/27 patients were treated with immune checkpoint inhibitors, including 10 cases having achieved clinical

complete remission, 2 cases with good response with stable disease, and 9 cases having succumbed to disease (follow-up 16-42 months).

Conclusions: Specific mutational signatures in hypermutated metastatic malignant tumors frequently correspond to certain tumor types and primary locations. These findings can facilitate investigation of tumor origins for metastases of unknown primary. In addition, considerable response rate to immune checkpoint inhibitor was observed in these cases. Larger scale clinical studies are needed to further establish the significance of the above observations.

893 Simultaneous Bright Field Chromogenic Multiplex Immunohistochemistry for the Next Generation of Companion Diagnostics

Faruk Erdem Kombak[1], Umesh Bhanot[1], Marina Asher[1], Irina Linkov[1], Adrian Murillo[2], Joachim Silber[1], Michael Roehrl[1]
[1]Memorial Sloan Kettering Cancer Center, New York, NY, [2]Ventana Medical Systems, Inc., Oro Valley, AZ

Disclosures: Faruk Erdem Kombak: *Speaker*, Roche; Umesh Bhanot: None; Marina Asher: None; Irina Linkov: None; Adrian Murillo: None; Joachim Silber: None; Michael Roehrl: None

Background: Multiplex immunohistochemistry is a powerful tool. We implemented bright field-based chromogenic pentaplex IHC with PD-L1, PD-1, CD3, CD8, and CD68 antibodies to better understand the tumor immune microenvironment and its relationship with IO checkpoint protein expression. We also developed 3 novel HRP-based chromogens as a prototype PD-L1 multiplex companion diagnostic using a triplex IHC design.

Design: The pentaplex design was tested on two TMA blocks containing a total of 87 pancreatic ductal adenocarcinoma cases, as well as three pan-cancer TMA blocks containing 144 tumors of various sites. Automated multiplex detection of proteins (PD-L1 (SP263), PD-1 (NAT105), CD3 (SP162), CD8 (SP57), and CD68 (KP-1)) using standard CC1 antigen-retrieved slides was accomplished on a Ventana Discovery Ultra. DAB (HRP) was used to visualize PD-L1, whereas Purple (HRP) for PD-1, Fast Red (AP) for CD68, Yellow (AP) for CD8, and Teal for CD3 were used.

The triplex design was tested on sections from various lung cancers. Automated triplex detection of PD-L1 (SP263), Cytokeratin (AE1/AE3), and TTF-1 (SPT24) was performed. The novel detection chromogens (Red HRP, Yellow HRP, and Blue HRP) utilize a tyramide-based, two-step, HRP-mediated process which results in the chromogen covalently depositing on the tissue. Yellow chromogen was matched with TTF-1, red with PD-L1, and blue with Cytokeratin.

Results: Immunoreactivity with DAB/PD-L1, Purple/PD-1, Fast Red/CD68, Yellow/CD8, and Teal/CD3 combinations in our pentaplex design was intense and selective (Figure 1). Staining was easily distinguishable with focally minimal background staining, even in areas of dense immune infiltrates with intermingled $CD3^+$ and $CD8^+$ T lymphocytes. Chromogen overlapping was not observed.

Figure 1 - 893

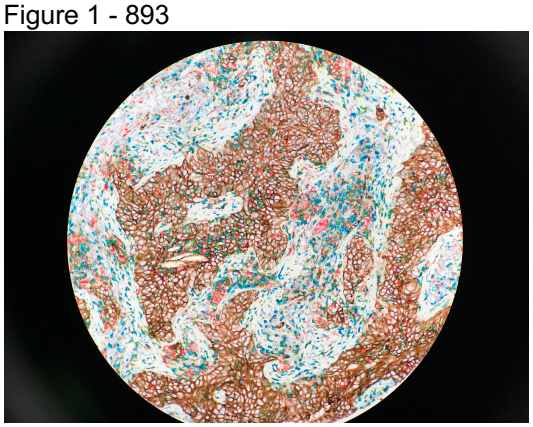

Conclusions: Multiplex chromogenic IHC is a powerful high-throughput tool that preserves tissue. It makes possible the precise assessment of more than one marker per section with the ability to reveal exact spatial context and proximity between cells and/or certain molecules. The automated platform in our use works based on simultaneous and sequential cycles using chromogens with broad absorbance spectra without destaining steps and does not need the integration of a scanner, imaging microscope, or analytic software. Evaluation of the staining can be easily performed with a conventional bright field microscope. Chromogenic multiplex IHC, as exemplified by our IO pentaplex and lung cancer triplex panels, is a powerful companion diagnostic for immune checkpoint inhibitor therapy guidance.

894 ILLUMINA TruSight Oncology 500 Sequencing Panel Validation at A Large Community Based Hospital

Sandeep Kumar[1], John Schwartz[1], Mitual Amin[2], Jennifer Kilbourn[1], Hlee Vue[1], Susan Daraiseh[1], Kausar Jabbar[1]
[1]Beaumont Health, Royal Oak, Royal Oak, MI, [2]William Beaumont Hospital, Royal Oak, MI

Disclosures: Sandeep Kumar: None; John Schwartz: None; Mitual Amin: None; Jennifer Kilbourn: None; Hlee Vue: None; Susan Daraiseh: None; Kausar Jabbar: None

Background: With growing efficacy of targeted therapy, it is critical to have comprehensive tumor profiling. TruSight Oncology 500 (TSO500) is a hybrid capture based next generation sequencing (NGS) assay that enables comprehensive genomic profiling of tumor samples. TSO500 includes 523 cancer-related genes which provides identification of pertinent single nucleotide variants (SNV), insertions and deletions (Indels), splice variants, fusions, copy number variants (CNV), tumor mutational burden (TMB) and microsatellite instability (MSI), from genomic DNA and RNA.

Design: We evaluated the performance of TSO500 using a combination of 102 formalin fixed paraffin embedded (FFPE) tumor types, 41 hematologic samples and 27 reference standard samples (Images 1A and 1B). The clinical samples were previously tested by reference laboratories using NGS. Test performance considered optimal with specimens containing at least 10% tumor cells, and nucleic acid concentration of at least 3.3 ng/µL for DNA and 4.6 ng/µL for RNA. Library preparation performed using hybrid capture based TruSight Oncology 500 Library Preparation Kit and sequenced on Nextseq 550/500. Sequenced data analyzed using TSO500 local app and analysis pipeline customized in collaboration with PierianDX.

Results: For clinical samples, SNVs with at least 3 % allele frequency and at least 100X depth of coverage detected with 97% sensitivity. Indels with 3% allele frequency and depth of coverage at least 100X detected with 95% sensitivity. CNVs with 3 or greater copies detected with 94% sensitivity. RNA fusions detected with 72% sensitivity. TMB values determined without the need for matched normal DNA. (Table 1)

Variant Type	Clinical Samples Only	Reference Standards & Clinical Samples
	Sensitivity	Sensitivity
SNV	97%	99%
Indels	95%	98%
CNVs	94%	98%
RNA Fusions	72%	92%

Figure 1 - 894

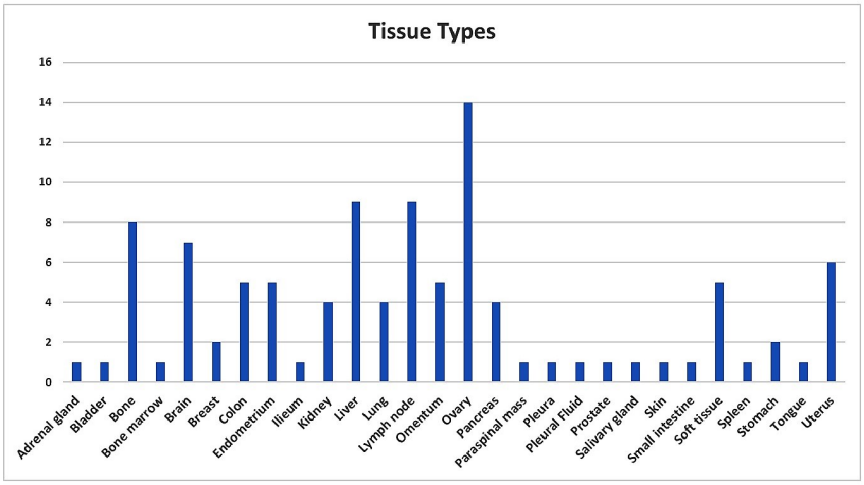

Image 1A: Solid Tumor Tissue Source of Extracted DNA and RNA used for TSO500 Assay.

Figure 2 - 894

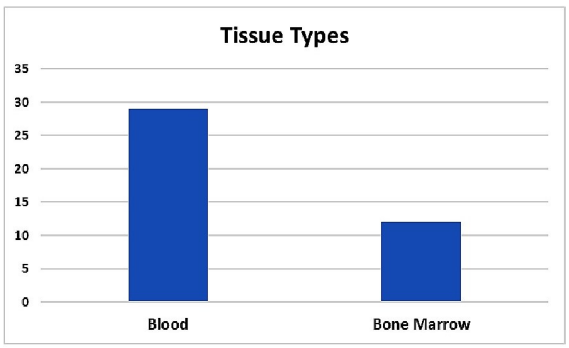

Image 1B: Hematologic Tissue Source of Extracted DNA and RNA used for TSO500.

Conclusions: Use of a large cancer panel, like TSO500, allows detailed and simultaneous assessment of SNVs, fusions, CNVs, in a single assay at low variant allele frequencies (VAFs) with a high degree of sensitivity and specificity. This comprehensive oncology panel can also assess biomarkers such as TMB and MSI, both of which are helpful in patients stratification for targeted and immune therapy.

895 FIBI: Novel, Direct-to-Digital, Slide-Free Histology for Rapid, High-Quality Imaging of Tissue Specimens

Richard Levenson[1], Farzad Fereidouni[2], Taryn Morningstar[1]
[1]UC Davis Health, Sacramento, CA, [2]University of California, Davis, Sacramento, CA

Disclosures: Richard Levenson: *Stock Ownership*, Histolix, Inc.; *Stock Ownership*, MUSE Microscopy Inc.; Farzad Fereidouni: *Stock Ownership*, HistoliX; Taryn Morningstar: None

Background: The traditional histology workflow in pathology, based on formalin-fixation, paraffin-embedding, microtomy, mounting on glass slides, staining and delivery for review, is now recognized as a logistical challenge, especially if the process has to be followed by whole-slide scanning to create a digital image. Frozen sections used for rapid tissue imaging, come with their own drawbacks. A method that can go directly from thick (unsectioned) tissue specimens, either fresh or fixed, to diagnostic-quality histology while skipping most of histology workflow,

would be desirable. A variety of methods are under development; here we present FIBI, a technique with speed, cost and quality properties that set it apart.

Design: FIBI (fluorescence imitating brightfield imaging) captures surface-weighted microanatomy from thick tissue with immediate resemblance to H&E-stained slides. The tissue specimen is stained with hematoxylin and eosin (30 seconds) and then immediately imaged using excitation in the visible range and a long-pass emission filter. The technique generates back-light-illumination that passes through the tissue surface layer stained with H&E. Imaging takes place via conventional frame-by-frame scanning, allowing the collection of 2 x 2 cm^2 regions at 10X magnification within a minute or two. 20X magnification is possible as well. AI tools for high-quality color mapping to generate very convincing images with H&E coloration can also be applied.

Results: We have imaged a wide variety of tissues, and the resemblance to standard histology is a general property. Shown here (Fig. 1) is a comparison of skin imaged either from a conventional histology slide, or by FIBI viewing a thick (1 mm) slice directly. The color space of FIBI images, while it bears a resemblance to authentic H&E staining, is not an exact match. We have developed cycleGAN (AI) unpaired imaging conversion tools to convert FIBI images to closely recapitulate typical H&E appearance. A comparison is shown in Fig. 2.

Figure 1 - 895

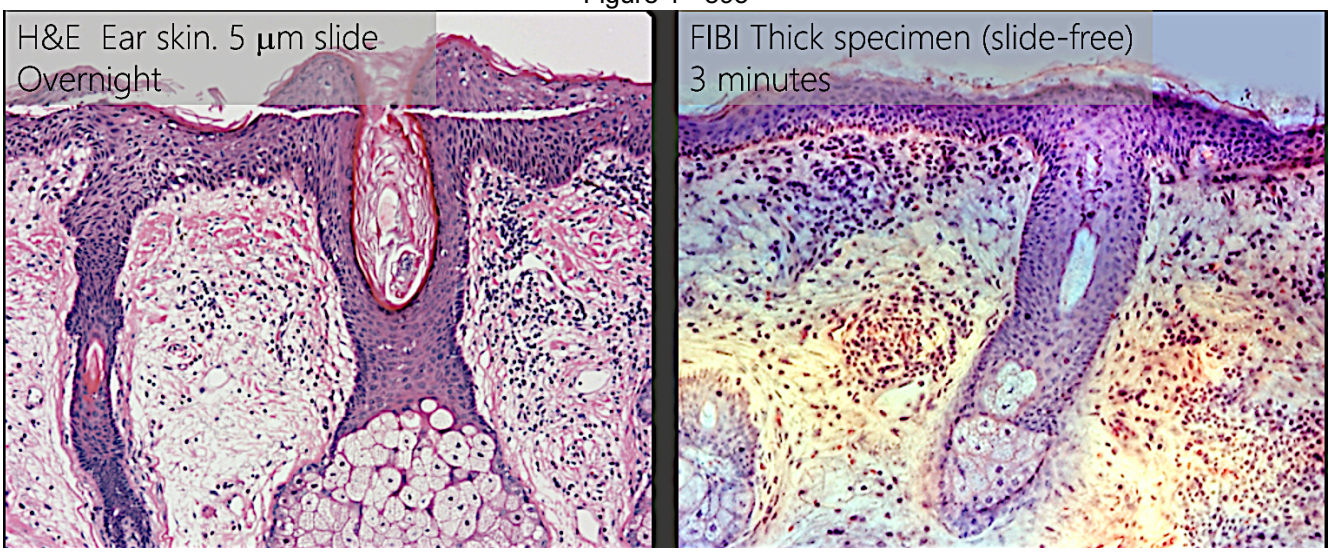

Figure 2 - 895

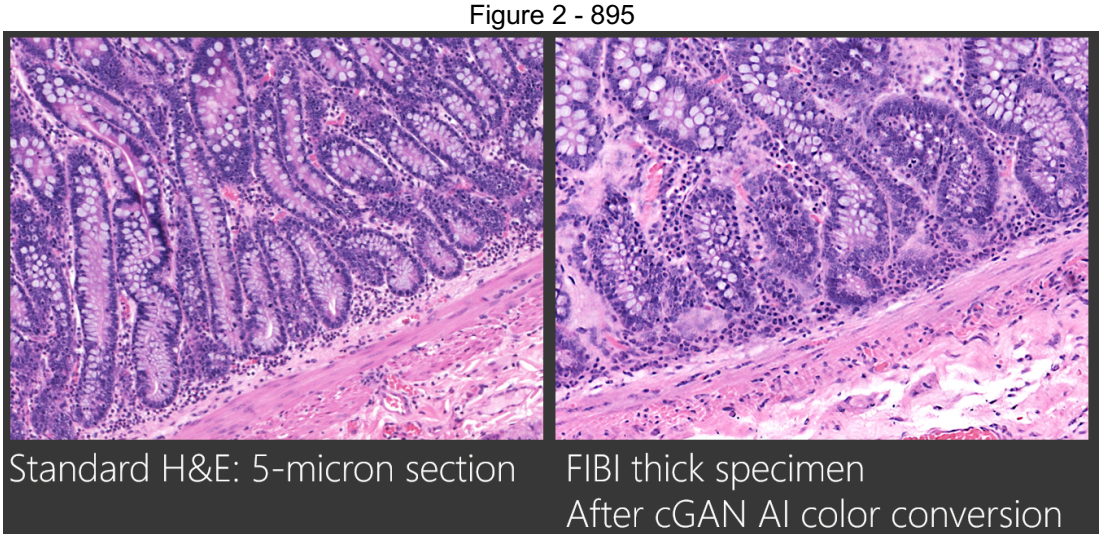

Conclusions: FIBI is a rapid, low-complexity, easy to use method for generating diagnostic-quality images directly from fresh or fixed, unsectioned tissues. It is non-destructive and leaves the specimen intact for long-term storage and/or submission for downstream molecular assays. It is a likely candidate to substitute for frozen sections, to provide ROSE evaluations of core-needle biopsies, and as a potential cost-reducer for general histology applications.

896 Ex Vivo Expansion of Circulating Tumour Cells (CTCs)

Bashir Mohamed[1], Mark Ward[2], Mark Bates[1], Tanya Kelly[1], Cathy Spillane[1], Cara Martin[3], Michael Gallagher[1], John Kennedy[1], Feras Abu Saadeh[4], Noreen Gleeson[4], Doug Brooks[5], Robert Brooks[5], Stavros Selemidis[6], Sharon O'Toole[3], John O'Leary[1]
[1]Trinity College Dublin, Dublin, Ireland, [2]Coombe Women & Infants University Hospital, Dublin, Ireland, [3]Trinity St. James's Cancer Institute, Dublin, Ireland, [4]St. James's Hospital, Dublin, Ireland, [5]University of South Australia, Adelaide, Australia, [6]RMIT, Mellbourne, Australia

Disclosures: Bashir Mohamed: None; Mark Ward: None; Mark Bates: None; Tanya Kelly: None; John Kennedy: None; Robert Brooks: None; Sharon O'Toole: None

Background: Circulating tumour cells (CTCs) play a crucial role in cancer dissemination and cellular extravasation leading to metastasis. There are only a limited number of CTCs per clinically/ethically allowed cancer patient`s blood draw and expanding this population of cells *in vitro* is crucial in order to provide a reliable number of cells to analyse CTC biology. CTCs can grow in a hypoxic environment and the activation of hypoxia-inducible factor (HIF-1α) results in increased cell survival and cellular proliferation, leading to cancer progression. Our aim was to optimise cell culture conditions using cobalt chloride ($CoCl_2$) as a chemical inducer of hypoxia that would allow us to examine growth of cells in real time. Primary ovarian cancer cells would be used for the hypoxia optimisation and conditions adapted ovarian/breast CTC cultures *in vitro*.

Design: Primary ovarian cancer cells were cultured in modified media supplemented with various concentrations of $CoCl_2$ for HIF1 α induction (50, 100, 150 and 200 uM). Cell viability and the expression of HIF-1α, PHH3, EpCAM and HER2 were examined in these cells using either ELISA, Immunoblotting or Immunofluorescence techniques. CTCs were isolated from breast and ovarian cancer patients using the ScreenCell® Cyto R device and cultured in specially modified media optimised for CTC culture supplemented with 20% FCS, growth factors and additives including: FGF-2, FGF-10, Nicotinamide, Y-27632, Primocin and $CoCl_2$. EpCAM and HER2 were examined in cultured and expanded CTCs using Immunofluorescence techniques.

Results: HIF-1α expression was induced and cell proliferation and viability were maintained in the primary ovarian cancer cells at a concentration of 100 µM of $CoCl_2$. Subsequently this concentration was used for the culturing of isolated CTCs. Using this condition, CTCs were successfully cultured and expanded for more than nine weeks. Based on the morphological and phenotypical characterisation, two phenotypes of CTCs were isolated from a breast cancer patient; epithelial-like expressed EpCAM and quasi-mesenchymal express HER2.

Conclusions: We demonstrated the feasibility of culturing cancer patient blood derived CTCs under hypoxic conditions. We also demonstrated the presence of heterogenous CTC populations; classical epithelial-like CTCs and quasi-mesenchymal subtypes in a breast cancer patient and their corresponding molecular phenotypes. Our work also demonstrated the suitability of size-based isolation for this culturing approach.

897 Clinical Utilization of Circulating Tumor DNA Analysis in the Management of Patients with Solid Tumors: A Single Institution's Experience

Michael Moravek[1], Lorenzo Gerratana[2], Neelima Katam[3], Firas Wehbe[2], Devalingam Mahalingam[2], Jeannine Donahue[3], Massimo Cristofanilli[2], Amir Behdad[2]
[1]Northwestern Memorial Hospital, Chicago, IL, [2]Northwestern University Feinberg School of Medicine, Chicago, IL, [3]Ann & Robert H. Lurie Children's Hospital of Chicago, Chicago, IL

Disclosures: Michael Moravek: None; Lorenzo Gerratana: *Consultant*, Novartis; *Advisory Board Member*, Eli Lilly; Neelima Katam: None; Devalingam Mahalingam: None; JEANNINE DONAHUE: None; Massimo

Cristofanilli: *Consultant*, Lilly; *Consultant*, Foundation Medicine; *Speaker*, Pfizer; *Consultant*, G1 therapeutics; *Consultant*, Sermonix; Amir Behdad: None

Background: Circulating tumor DNA (ctDNA) is becoming an instrumental tool in the practice of precision oncology, but there is broad variability in its utilization. In this study we describe the findings from our large cohort of clinical ctDNA tests to further guide our ctDNA utilization in various solid tumors.

Design: We evaluated the results of all Guardant360 ctDNA tests that were performed in patients with a variety of solid tumors from June 2014 to July 2020. A total of 23 tumor categories were analyzed. We determined the frequency of identifying clinical trials and FDA approved medications for each tumor category. We determined the most common genomic alterations and variant allele frequencies for each tumor category. In addition, we compared the results of ctDNA with tumor next generation sequencing (tNGS) for most commonly mutated genes in various tumor types.

Results: A total of 3198 tests for 1763 patients were performed with 30% of patients tested more than once. The most common tumors included breast carcinoma (BC) (1455 tests), lung adenocarcinoma (LAC) (750 tests), and colorectal adenocarcinoma (CRC) (408 tests). In 83% of patients, at least one test identified a somatic alteration. The most common mutated gene in all types of tumors was TP53 followed by PIK3CA and ESR1 mutations in BC, KRAS and EGFR mutations in NSCLC and APC and KRAS in CRC (a summary of data is available in Table 1). The highest variant allele frequencies were seen in CRC. Based on the genomic alterations an FDA-approved targeted therapy was available in 16.4% of cases (22% in BC, 20% in LAC) and a clinical trial was available in 67% of patients (90% in CRC, 70% in LAC and 60% in BC). The agreement between blood and tissue sequencing was >80% for driver mutations in most types of tumors, but the highest degree of agreement was seen for mutations in LAC (kappa=0.7).

Breast Carcinoma		Lung Adenocarcinoma		Colorectal Carcinoma		Pancreatic Cancer		Lung Squamous Cell Carcinoma		Lung Small Cell Carcinoma		Cholangiocarcinoma		Prostate Adenocarcinoma		Ovarian Carcinoma		Endometrial Carcinoma		Carcinoma of Unknown Primary		Thyroid Carcinoma	
TP53_mut	48%	TP53_mut	52%	APC-mut	71%	TP53_mut	64%	TP53_mut	75%	TP53_mut	65%	TP53_mut	46%	TP53_mut	40%	TP53_mut	76%	TP53_mut	83%	TP53_mut	50%	TP53_mut	30%
PIK3CA-mut	25%	KRAS-mut	21%	TP53_mut	70%	KRAS-mut	61%	PIK3CA-amp	17%	RB1-mut	30%	IDH1-mut	13%	AR-amp	34%	PIK3CA-amp	18%	PIK3CA-mut	38%	KRAS-mut	19%	KRAS-mut	7%
ESR1-mut	18%	EGFR-mut	20%	KRAS-mut	51%	CDKN2A-mut	10%	EGFR-amp	11%	PIK3CA-amp	30%	KRAS-mut	11%	MYC-amp	24%	PIK3CA-mut	9%	PTEN-mut	21%	PIK3CA-mut	15%	ARID1A-mut	4%
FGFR1-amp	13%	PIK3CA-mut	5%	EGFR-amp	20%	SMAD4-mut	9%	PIK3CA-mut	9%	ERBB2-amp	16%	PIK3CA-mut	9%	BRAF-amp	21%	KRAS-mut	9%	ARID1A-mut	17%	RB1-mut	15%	BRAF-mut	4%
MYC-amp	13%	BRAF-mut	5%	PIK3CA-mut	20%	PIK3CA-amp	9%	KRAS-mut	9%	NF1-mut	14%	TERT-mut	9%	EGFR-amp	18%	ARID1A-mut	9%	KRAS-mut	13%	PIK3CA-amp	12%	MET-mut	4%
CCND1-amp	10%	STK11-mut	5%	BRAF-amp	11%	ERBB2-amp	8%	NFE2L2	9%	BRAF-amp	14%	MYC-amp	9%	CDK6-amp	18%	MYC-amp	9%	PIK3CA-amp	13%	EGFR-amp	12%	NF1-mut	4%
EGFR-amp	9%	PIK3CA-amp	4%	CDK6-amp	10%	MYC-amp	7%	MET-amp	8%	KRAS-amp	11%	APC-mut	4%	PIK3CA-amp	16%	KIT-amp	9%	FGFR1-amp	13%	BRAF-amp	12%	KIT-mut	4%
ERBB2-amp	9%	CCNE1-amp	4%	SMAD4-mut	9%	ARID1A-mut	5%	PTEN-mut	7%	CCNE1-amp	11%	ERBB2-mut	4%	FGFR1-amp	15%	PDGFRA-amp	9%	MYC-amp	13%	MET-amp	12%	FGFR2-mut	4%
CCNE1-amp	8%	NF1-mut	4%	MYC-amp	9%	PIK3CA-mut	4%	BRAF-amp	7%	CCND2	8%	ARID1A-mut	4%	MET-amp	13%	APC-mut	6%	CCNE1-amp	13%	CCNE1-amp	12%	GNAS-mut	4%
PIK3CA-amp	8%	CDKN2A-mut	4%	BRAF-mut	8%	BRCA2-mut	4%	MYC-amp	7%	CDK4	8%	BRAF-mut	4%	AR-mut	11%	BRCA1-mut	6%	GNAS-mut	8%	ARID1A-mut	8%	NRAS-mut	4%
BRAF-amp	7%	MYC-amp	4%	NRAS-mut	7%	ATM-mut	4%	CDK6-amp	7%	EGFR-mut	5%	MET-mut	4%	KIT-amp	11%	KRAS-amp	6%	CTNNB1	8%	NF1-mut	8%	MAP2K1	4%
CDK6-amp	7%	CDK4	3%	FGFR1-amp	7%	ERBB2-mut	3%	NF1-mut	5%	KIT-mut	5%	FGFR2-mut	4%	APC-mut	10%	BRAF-amp	6%	ERBB2-amp	8%	PTEN-mut	8%	IDH2	4%
PTEN-mut	7%	ATM-mut	3%	ARID1A-mut	7%	MET-amp	3%	BRCA2-mut	5%	MET-amp	5%	PTEN-mut	4%	PIK3CA-mut	8%	CCNE1-amp	6%	BRAF-amp	8%	SMAD4-mut	8%	CCDC6-RET	4%
ARID1A-mut	5%	RB1-mut	3%	PIK3CA-amp	7%	CDK6-amp	3%	CDKN2A-mut	5%	FGFR1-amp	5%	GNAS-mut	4%	BRCA2-mut	8%	BRAF-mut	3%	FGFR2-amp	8%	CDKN2A-mut	8%	RET-CCDC6	4%
GNAS-mut	4%	GNAS-mut	3%	MET-amp	7%	CCND1-amp	3%	STK11-mut	5%	MYC-amp	5%	EGFR-mut	2%	PDGFRA-amp	8%	NF1-mut	3%	RAF1	8%	FGFR1-amp	8%	PIK3CA-amp	4%
KRAS-mut	4%	SMAD4-mut	3%	GNAS-mut	6%	BRAF-mut	2%	FGFR1-amp	5%	CDK6-amp	5%	NF1-mut	2%	CCNE1-amp	6%	BRCA2-mut	3%	APC-mut	4%	CDK6-amp	8%	BRAF-amp	4%
ERBB2-mut	4%	CTNNB1	3%	NF1-mut	5%	PTEN-mut	2%	CCNE1-amp	5%	CCND1-amp	5%	BRCA2-mut	2%	CCND1-amp	6%	ATM-mut	3%	ERBB2-mut	4%	RAF1	8%	CDK6-amp	4%
BRCA2-mut	4%	EGFR-amp	3%	ATM-mut	4%	NRAS-mut	2%	CCND1-amp	5%	KRAS-mut	3%	FGFR1-mut	2%	RAF1	6%	KIT-mut	3%	MET-mut	4%	ERBB2-mut	4%		
GATA3-mut	4%	CDK6-amp	3%	ERBB2-amp	4%	EGFR-amp	2%	EGFR-mut	4%	APC-mut	3%	ATM-mut	2%	NF1-mut	5%	FGFR2-mut	3%	NF1-mut	4%	TERT-mut	4%		
NF1-mut	4%	APC-mut	2%	EGFR-mut	4%	KRAS-amp	2%	ARID1A-mut	4%	ARID1A-mut	3%	RB1-mut	2%	PTEN-mut	5%	NOTCH1-mut	3%	BRCA2-mut	4%	STK11-mut	4%		
RB1-mut	4%	ARID1A-mut	2%	CCND2	4%	BRAF-amp	2%	RB1-mut	4%	MET-mut	3%	SMAD4-mut	2%	CTNNB1	5%	RB1-mut	3%	ATM-mut	4%	GNAS-mut	4%		
ATM-mut	3%	MET-mut	2%	FBXW7-mu	3%	CCND2	2%	KRAS-amp	4%	BRCA2-mut	3%	CDKN2A-mut	2%	KRAS-mut	3%	GNAS-mut	3%	CDK6-mut	4%	IDH1-mut	4%		
BRCA1-mut	3%	EML4-ALK	2%	BRCA2-mut	2%	APC-mut	1%	ERBB2-amp	4%	ATM-mut	3%	FBXW7	2%	BRAF-mut	3%	MTOR-mut	3%	FGFR2-mut	4%	NFE2L2	4%		

Conclusions: This retrospective analysis of large cohort of patients with diverse varieties of solid tumors reveals that ctDNA is very likely to reveal the genomic composition of tumors and is a reliable method to guide precision therapy.

898 Deep Proteomic and Phosphoproteomic Analysis of NSCLC EGFR-TKI-Resistance Mechanisms

Kei Namba[1], Atsushi Tanaka[1], Makiko Ogawa[1], Ronald Hendrickson[1], David Klimstra[1], Shinichi Toyooka[2], Michael Roehrl[1]
[1]Memorial Sloan Kettering Cancer Center, New York, NY, [2]Okayama University, Okayama, Japan

Disclosures: Kei Namba: None; Atsushi Tanaka: None; Makiko Ogawa: None; Ronald Hendrickson: None; David Klimstra: None; Shinichi Toyooka: None; Michael Roehrl: None

Background: Kinase inhibitors, especially tyrosine kinase inhibitors (TKIs), have been developed as anti-cancer drugs, but drug resistance remains an obstacle in clinical practice. Why cancer cells that are otherwise seemingly identical at DNA/RNA levels can be either resistant or susceptible to TKIs remains a mystery. In this study, we conducted a comprehensive comparison of drug-resistant vs. genomically matched drug-sensitive parental non-small cell lung cancer (NSCLC) cells using proteomics to discover resistance-associated proteins and pathways.

Design: We established acquired osimertinib-resistant cell lines from EGFR-mutant NSCLC cells using two different procedures: stepwise drug escalation exposure and high-concentration intermittent drug exposure. Proteins were extracted from sensitive parent and resistant cell lines, and global deep proteomics and phosphoproteomics were performed by liquid chromatography-mass spectrometry. Protein identification and signature profiling were carried out with Perseus software. We performed differential expression analyses and protein pathway enrichment analyses using Metascape. We searched drug-proteins interactions in the drug-gene interaction database (DGIdb) for putative new drug targets.

Results: Using Tandem Mass Tag-Synchronous Precursor Section-MS^3, over 9,000 protein IDs and over 5,000 phosphoprotein IDs were detected. In a comparative analysis of parental and resistant cell lines, several key signaling pathways were upregulated/downregulated in resistant cell lines, showing that cancers can use functional biochemical changes to acquire resistance phenotypes. We identified inhibitory drugs in a DGIdb search that may overcome resistance.

Conclusions: Deep proteomics and phosphoproteomics combined with pathway analyses revealed biomarkers and pathways of resistance, suggesting promising therapeutic strategies for overcoming induced TKI resistance in NSCLC. More broadly, proteome-based diagnostics of lung cancer holds great promise and is able to explain drug resistance mechanisms that are invisible to nucleic acid-based diagnostics.

899 Clinical Validation of Tumor Mutational Burden (TMB) in Solid Tumors by NGS: Impact of Revised TMB-High Threshold

Vamsi Parimi (Parini)[1], Rena Xian[2], Ming-Tseh Lin[3], James Eshleman[1], Christopher Gocke[4], Aparna Pallavajjala[4]
[1]Johns Hopkins University School of Medicine, Baltimore, MD, [2]Johns Hopkins Medical Institutions, Baltimore, MD, [3]Johns Hopkins Hospital, Baltimore, MD, [4]Johns Hopkins University, Baltimore, MD

Disclosures: Vamsi Parimi (Parini): None; Rena Xian: None; Ming-Tseh Lin: None; James Eshleman: None; Christopher Gocke: None; Aparna Pallavajjala: None

Background: Tumor mutation burden (TMB) is a clinical predictive biomarker for immune checkpoint blockade. Our validation is aimed to construct a next-generation sequencing (NGS) analysis pipeline for calculation of TMB that would perform on par with an FDA approved TMB assay.

Design: A test cohort consisting of tumor only samples (n=211) and NCI-60 cell lines (n=11) and a validation cohort (n=705) were used for estimation of TMB. All of these samples had minimum tumor cellularity ≥ 20% and mean sequencing depth ≥ 300X. TMB values derived from a 432-gene (1.1374 Mb) panel were compared with concurrent TMB data generated by an FDA approved assay (FM-TMB based on FoundationOneCDx assay) and with concurrent data generated from a TMB harmonization study (FOCR Phase I). TMB-eligible variants were defined as: minimum VAF of 5%, ≥50x allele-specific sequencing depth. Coding and splice site variant calls were excluded if they were likely germline origin based on dbSNP and the Somatic-Germline-Zygosity (SGZ) algorithm, and if they were also identified in a pool of normal negative control samples (n=16). TMB-eligible variants were

then summed as total mutations/Mb. Performance characteristics of the TMB algorithm were developed from the test cohort, validated using the validation cohort, and compared against the TCGA MC3 data set (n=4134).

Results: Our algorithm (MDLVCv7) showed a significant positive correlation with TCGA's WES TMB (R2= 0.983). In the test cohort, orthogonal *in silico* comparison of our TMB (JH-TMB) calculation with FM-TMB calculations achieved an overall correlation coefficient of 0.913. Also, there was no significant difference between JH-TMB and FM-TMB interpretation (2 tailed Wilcoxon Signed Rank Test; P=0.53). The clinically meaningful TMB-high (TMBh) threshold has recently been changed from 20 to 10. At those levels, the sensitivity, specificity and accuracy of JH algorithm compared to FM-TMB for TMBh ≥20 and ≥10 are 100%, 99.5%, 99.5% (95%CI: 97.4% - 99.99%) and 89%, 87% and 87% (95%CI: 82.50% - 91.33%), respectively. Changing TMBh from ≥20 to ≥10 reclassified 5.3% of cases. The correlation of MSI-H/dMMR cases with TMBh (≥10) was 100% among a subset of the validation cohort.

Figure 1 - 899

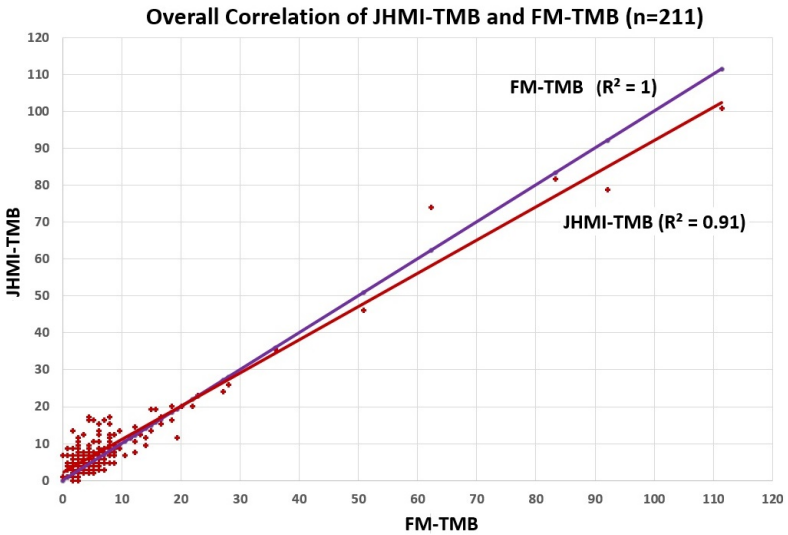

Figure 2 - 899

Performance Characteristics of JHMI-TMBh with FM-TMB as Reference (n=211)				
	TMBh (≥10)		TMBh (≥20)	
Statistic	Value	95% CI	Value	95% CI
Sensitivity	100.00%	71.51% to 100.00%	89.29%	71.77% to 97.73%
Specificity	99.50%	97.25% to 99.99%	87.14%	81.85% to 91.35%
Positive Likelihood Ratio	200	28.31 to 1412.92	6.94	4.77 to 10.10
Negative Likelihood Ratio	0	NA	0.12	0.04 to 0.36
Disease prevalence (*)	5.21%	2.63% to 9.14%	11.76%	7.96% to 16.55%
Positive Predictive Value (*)	91.67%	60.89% to 98.73%	48.08%	38.89% to 57.39%
Negative Predictive Value (*)	100.00%	NA	98.39%	95.44% to 99.44%
Accuracy (*)	99.53%	97.39% to 99.99%	87.39%	82.50% to 91.33%

Conclusions: We have successfully implemented a TMB algorithm without germline tissue sequencing capturing 100% of MSI-H/dMMR cases as TMBh, and demonstrating high correlation to reference TMBs obtained by WES and an FDA approved assay.

900 The Utility of NGS as a Functional Assay to Diagnose dMMR and the Implication of dMMR Status to the Overall TMB Score

Vamsi Parimi (Parini)[1], Aparna Pallavajjala[2], Rena Xian[3], Christopher Gocke[2], Ming-Tseh Lin[4], James Eshleman[1]

[1]Johns Hopkins University School of Medicine, Baltimore, MD, [2]Johns Hopkins University, Baltimore, MD, [3]Johns Hopkins Medical Institutions, Baltimore, MD, [4]Johns Hopkins Hospital, Baltimore, MD

Disclosures: Vamsi Parimi (Parini): None; Aparna Pallavajjala: None; Rena Xian: None; Christopher Gocke: None; Ming-Tseh Lin: None; James Eshleman: None

Background: Tumor mutation burden (TMB) is a clinical predictive biomarker for immune checkpoint blockade. Germline or sporadic DNA mismatch repair deficiency (dMMR) is known to cause a mutator phenotype often contributing to high tumor mutational burden (TMBh). We evaluated the specific alterations that are unique to functional repair defect of MMR genes (MLH1, MSH2, MSH6, and PMS2) by Next Generation Sequencing (NGS). We aimed to quantify the contribution of dMMR to the overall TMB score which would act as an internal control during the clinical validation of TMB.

Design: 825 solid tumors with a known mismatch repair deficiency status underwent 432-gene (1.1374 Mb) NGS solid tumor only assay. dMMR is defined as loss of MMR proteins by immunohistochemical stains and/or MSI-high status by the MSI assay. TMB is clinically validated using WES (FOCR Phase I TMB harmonization study) and FDA approved assay (FM-TMB, FoundationOneCDx assay) without germline tissue sequencing. TMB-eligible variants are defined as: minimum VAF of 5%, ≥50x allele-specific sequencing depth. Coding and splice site variant calls are excluded if they were likely germline origin based on dbSNP and the Somatic-Germline-Zygosity (SGZ) algorithm. TMB is calculated as the sum of eligible mutations/Mb.

Results: Orthogonal *in silico* comparison of our TMB calculation with FM-TMB calculations achieved a correlation coefficient of 0.913. The TMB score is significantly higher in 79 (9.5%) dMMR cases (mean+SD: 45+60, range: 11-449) as compared to the 746 MMR proficient (pMMR) cases (4.79±15, range: 0-233) (Fig 1: Violin plot). Among pMMR cases, 36 (5%) had TMB>10. The ratio of nonsynonymous to synonymous mutations among dMMR cases is 2.64. The single most characteristic single base substitution signature among dMMR is A>G (T>C) at 31 % (COSMIC signature 26) (Fig 2: Histogram). The average frameshift deletions and insertion mutations per dMMR case is 6.7±4 (range: 1-19) and 3.4±2.6 (range: 1-12), respectively.

Figure 1 - 900

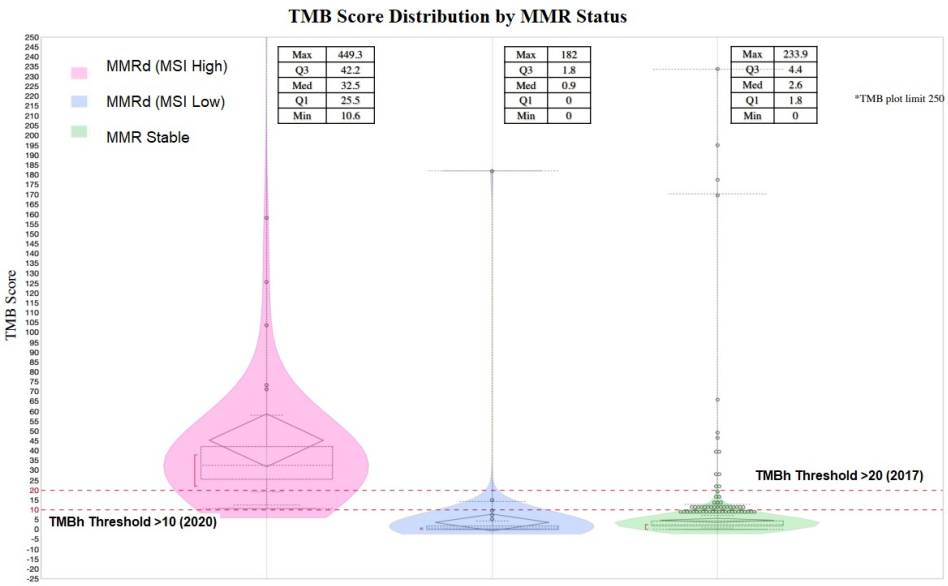

Figure 2 - 900

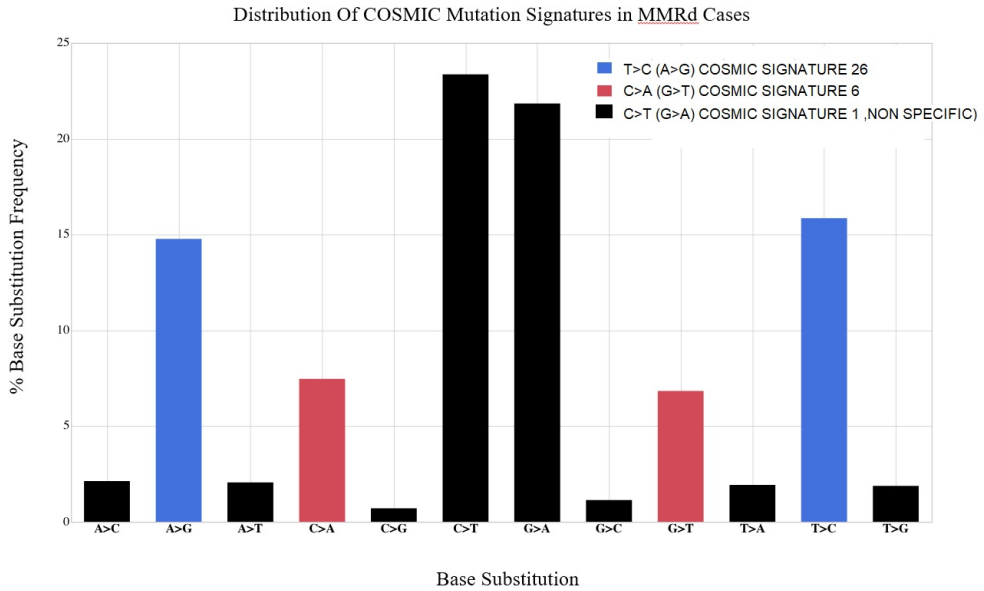

Conclusions: dMMR is the single most common phenomenon seen among TMBh cases. We report a significant increase in the TMB score among dMMR cases compared to pMMR cases. We report the diagnostic utility of NGS as a functional assay based on a unique mutation signature in dMMR cases to test for germline or sporadic DNA mismatch repair deficiency.

901 Determination of Microsatellite Instability Using a Custom Designed Next Generation Sequencing Panel for Comprehensive Clinical Testing and Personalized Cancer Treatment

Ramakrishna Sompallae[1], Krishnaveni Sompallae[1], Natalya Guseva[2], Rachel Starks[1], Aaron Bossler[2], Deqin Ma[1]
[1]University of Iowa Hospitals & Clinics, Iowa City, IA, [2]University of Iowa, Iowa City, IA

Disclosures: Ramakrishna Sompallae: None; Krishnaveni Sompallae: None; Natalya Guseva: None; Rachel Starks: None; Aaron Bossler: None; Deqin Ma: None

Background: Microsatellite instability (MSI) is used to identify patients with Lynch syndrome and to determine patient's eligibility for immune checkpoint inhibitors. In metastatic colon cancer, mutation analysis of *RAS* and *BRAF* is required for predicting response to anti-EGFR therapy and prognosis. The majority laboratories still use immunohistochemistry (IHC) for DNA mismatch repair proteins (MMR), PCR-based testing for MSI, and next generation sequencing (NGS) for detecting *RAS* and *BRAF* mutations. We implemented a custom designed, 215-gene NGS panel for comprehensive genomic analysis including single nucleotide variants (CNV), small deletion insertion (delins), and copy number variations (CNV). In this study, we assessed the ability of this panel to detect MSI and compared the results from MMR and PCR.

Design: Microsatellite testing was performed on 21 cases [15 MSI-high (MSI-H) and 6 MS-stable (MSS)] that were previously tested by IHC and/or PCR. Libraries prepared from genomic DNAs of patient tumors were sequenced on the NextSeq instrument (Illumina) using a custom designed, Ampliseq-based, 215-gene panel (~750 Kbp). Over 300 microsatellite markers were identified in this custom NGS panel using the MANTIS program (Kautto EA, et al. Oncotarget. 2017. 8(5); 7452-7463). MSI-H tumor/normal pairs were initially evaluated to identify 25 markers with high ability to differentiate MSI. Using the MSIsensor-pro algorithm which does not require paired normals (Jia P, et al. Genomics Proteomics Bioinformatics. 2020 18:65–71), a read depth baseline was established for the 25 core markers on MSS specimens before evaluating the 21 test cases.

Results: All of the MSI-H calls from NGS testing (15/15) were concordant with the MSI status determined by PCR or IHC. The percentage of unstable sites ranged from 44-92% by NGS and were all greater than the NCI recommended cutoff for unstable sites of 30%. MSS specimens demonstrated 0-2 markers unstable. Table 1.

Table 1. Correlation of MSI Status Determined by PCR, IHC, and NGS

Case	MSI Status by PCR/IHC	%(#) Unstable Sites by NGS	Concordance of NGS with IHC/PCR
1	MSI-H	80 (20)	True positive
2	MSI-H	88 (22)	True positive
3	MSI-H	88 (22)	True positive
4	MSI-H	56 (14)	True positive
5	MSI-H	80 (20)	True positive
6	MSI-H	84 (21)	True positive
7	MSI-H	88 (22)	True positive
8	MSI-H	84 (21)	True positive
9	MSI-H	44 (11)	True positive
10	MSI-H	84 (21)	True positive
11	MSI-H	92 (23)	True positive
12	MSI-H	84 (21)	True positive
13	MSI-H	76 (19)	True positive
14	MSI-H	80 (20)	True positive
15	MSI-H	68 (17)	True positive
16	MSS	0 (0)	True positive
17	MSS	4 (1)	True negative
18	MSS	0 (0)	True negative
19	MSS	4 (1)	True negative
20	MSS	8 (2)	True negative
21	MSS	4 (1)	True negative

Conclusions: This custom designed NGS panel can reliably detect MSI status and allows for more efficient use of patients' specimens by combining it with detection of SNV, delins, and CNV. Since no normal tissue is required and no separate MSI test is needed, this assay reduces the cost and improves workflow.

902 NTRK Testing Practice in German Pathologies

Veronika Weyerer[1], Nadina Ortiz-Brüchle[2], Melanie Demes[3], Oliver Schildgen[4], Johannes Haybaeck[5], Gabriela Westphal[6], Philip Sander[7], Thomas Mairinger[8], Wolfgang Goering[9], Thomas Aigner[10], Udo Siebolts[11], Annika Moske[12], Achim Battmann[13], Hans Michael Kvasnicka[14], Karsten Neumann[15], Lars Tharun[16], Daniela Nussbeck[17], Marianna Sciortino[17], Bruno Markl[18], Eva Wardelmann[19], Arndt Hartmann[20], Nikola Holtkamp[17]

[1]University Hospital Erlangen, Friedrich-Alexander Universität Erlangen-Nürnberg, Frankfurt, Germany, [2]Institute of Pathology, RWTH Aachen University, Aachen, Germany, [3]Frankfurt, Germany, [4]Köln, Germany, [5]Innsbruck, Austria, [6]Klinikum Kassel, Kassel, Germany, [7]Tübingen University Hospital, Tübingen, Germany, [8]Berlin, Germany, [9]Heinrich-Heine University and University Hospital of Duesseldorf, Düsseldorf, Germany, [10]Coburg, Germany, [11]Universitaetsklinik Halle, [12]MVZ für Histologie, Zytologie und Molekular Diagnostik, Trier, Germany, [13]Institut fur Pathologie, Germany, [14]University of Witten/Herdecke, Witten, Germany, [15]Städtisches Klinikum Dessau, Dessau, Germany, [16]Pathology of the University Hospital Schleswig-Holstein, Campus Luebeck, Luebeck, Germany, [17]Diaceutics, Inc., Belfast, United Kingdom, [18]Institut fur Pathologie, [19]Universitaetsklinikum Muenster, Pathologie, Muenster, Germany, [20]Institut fur Pathologie, Erlangen, Germany

Disclosures: Veronika Weyerer: None; Gabriela Westphal: None; Philip Sander: None; Annika Moske: None; Hans Michael Kvasnicka: None; Lars Tharun: None; Marianna Sciortino: None

Background: The development and launch of first-generation neurotrophic tropomyosin receptor kinase (NTRK) inhibitors has brought targeted treatment options to *NTRK* fusion–positive adult and pediatric cancer patients who may have been out of treatment options. Adoption of *NTRK* fusion testing is crucial to support selection of patients for these small molecule inhibitors. Several methods and testing algorithms have been proposed for the detection

of *NTRK1-3* gene fusions. Here we determined how German pathologies approached *NTRK* gene fusion testing in 2019.

Design: 18 German pathologies including 11 academic, 6 public hospitals and one private institution provided information on accreditation, technologies, devices, consumables and *NTRK* testing algorithms employed. Moreover, volumes per tumor entity were provided by 12 labs. Monitoring of participating pathologies in respect to tumor volumes per entity and amendments in testing algorithms and technologies is ongoing in 2020.

Results: Sixteen out of 18 participants performed *NTRK* gene fusion testing in clinical routine in 2019. Fourteen labs were either certified or accredited and 17 labs had NGS devices available. A multitude of different testing algorithms was employed. Most frequently used testing approaches were NGS as only screening method (31%) and immunohistochemistry as pre-screening followed by NGS (19%). The most commonly employed NGS panels were Oncomine Comprehensive and Oncomine Focus Assay. Laboratory turnaround times were fast, with more than 50% of labs reporting results within 10 working days. For *NTRK* expression analysis by IHC labs mainly used the Abcam antibody and Ventana pan-TRK kit. FISH and RT-PCR were less commonly used in the clinical routine. A broad spectrum of different tumor types was tested for *NTRK* alterations with lung cancer being the most frequently analyzed tumor entity followed by colorectal cancer and melanoma.

Conclusions: The majority of 18 large German pathologies implemented clinical *NTRK* fusion testing before December 2019. In the first quarter of 2020 all participating pathologies had implemented in-house *NTRK* analysis. Utilization of different methodologies and testing algorithms is still providing a challenge and may affect the rate of patients identified with *NTRK* fusions.